The following publication H. Zheng, Y. Yan, Y. Wang, X. Shen and C. Lu, "Deep Learning Enhanced Long-Range Fast BOTDA for Vibration Measurement," in Journal of Lightwave Technology, vol. 40, no. 1, pp. 262-268, Jan.1, 2022 is available at https://doi.org/10.1109/JLT.2021.3117284.

Deep learning enhanced long-range fast BOTDA for vibration measurement

Hua Zheng, Yaxi Yan, Yuyao Wang, Xingliang Shen, and Chao Lu

***Abstract*—In this paper, we propose and experimentally demonstrate a scheme of deep learning enhanced long-range fast Brillouin optical time-domain analysis (BOTDA). The volumetric data from fast BOTDA is denoised and demodulated by using a deep video denoising network and a deep neural network, respectively. Benefitting from the advanced deep learning algorithms, the sensing range of fast BOTDA is extended to 10 km successfully. In experiment, vibration signal is measured with a sampling rate of 23 Hz, 2 m spatial resolution, and 1.19 MHz accuracy over 10 km single-mode fiber with only 4 averages. Due to the low computational complexity and GPU acceleration, the network takes less than 0.04 s to process 100×21800 data, which is much faster than the conventional algorithms. This method provides the potential for real-time vibration measurement in fast BOTDA with long sensing range.**

***Index Terms*—Brillouin optical time-domain analysis (BOTDA), deep learning, ultra-fast measurement**

I. Introduction

DISTRIBUTED optical fiber sensors (DOFS) possess the capability of continuously measuring the spatial map of environmental quantities that can be potentially applied in various fields such as structural health monitoring, pipeline safety warning, and power generation system monitoring [1]–[3]. As one of the typical Brillouin scattering based DOFS, Brillouin optical time-domain analysis (BOTDA) involves a pulsed pump and a CW probe counter-propagating in an optical fiber, interacting with each other through the acoustic wave. By measuring the Brillouin gain spectrum along the fiber, the environmental information can be spatially resolved [4]–[6]. BOTDA has advantages of high spatial resolution, long sensing distance, and large dynamic strain measurement range. However, the acquisition process of BOTDA is quite time-consuming, since the Brillouin gain spectrum (BGS) needs to map step by step over a wide frequency range and a large number of averaging is required to enable a desirable SNR. To solve this problem, numerous dynamic sensing techniques have been presented. Among them, slope-assisted BOTDA [7]–[10], sweep free BOTDA [11]–[13], and optical chirp chain BOTDA [14]–[16] omit the frequency sweeping process and thus can substantially boost the sensing speed. Alternatively, as one of the typical techniques to improve the sensing speed of BOTDA, fast BOTDA utilizes frequency-agile to reduce frequency switching time [17]–[19]. Acquisition rates up to several thousand hertz have been demonstrated, while the sensing range is only several hundred meters. With the increase of sensing distance, the SNR of signal decrease, number of averaging rather than frequency switching time become a dominant factor to deteriorate the sensing speed of fast BOTDA.

To extend the sensing distance of fast BOTDA, cyclic coding is employed to enhance the SNR, sensing speed of 440 Hz is achieved over ~2 km single-mode fiber [20]. Alternately, denoising algorithms could also improve the SNR of BOTDA without adding any hardware complexity. Several two-dimensional (2D) or three-dimensional (3D) image (video) denoising methods, which exploit redundancies and correlations contained in the multidimensional data, have been proposed [21]–[27]. The SNR of the sensor was demonstrated to be greatly improved by employing non-local means (NLM), wavelet denoising (WD), Block-Matching and 3D filtering (BM3D), and video BM3D. These conventional image denoising algorithms could enhance the sensing performance of BOTDA, however, generally involve complex optimization problems in the denoising procedure. Thus, these methods are time-consuming which cannot be used for real-time processing. In contrast, deep-learning based image denoising methods require extensive computation only during training. Once the network is well trained, it can be applied to perform real-time denoising. In 2018, the denoising convolutional neural network (DnCNN) was demonstrated to be effective for processing BOTDA signals with high data fidelity [28]. A 151 × 50000 size image can be effectively denoised in 0.045 s using GPU. Moreover, a Brillouin frequency shift (BFS) extraction convolutional neural network (BFSCNN) was also developed to extract BFS directly from the 2D data [29].

Compared with conventional BOTDA, fast BOTDA acquires BGSs with a much higher sampling rate, the collected data naturally features a strong coherence along the temporal axis. In this paper, we apply a fast deep video denoising network (fastDVDnet) to process the 3D fast BOTDA data. By using volumetric (i.e. spatio-temporal) image data, the temporal redundancy in adjacent data is well exploited. An SNR improvement of 10.85 dB is achieved via the trained fastDVDnet. Combining with the demodulating deep neural network (DNN), distributed dynamic strain sensing is achieved over 10 km single-mode fiber with 2 m spatial resolution and 1.19 MHz accuracy. Vibration signal is successfully measured with a sampling rate of 23 Hz. Besides, the network only takes 0.038 s (0.038 s for denoising and 0.001 s for BFS extracting)

This work was supported by General Research Fund PolyU 15209919 of the Hong Kong SAR government and project ZVGB of the Hong Kong Polytechnic University. (Corresponding author: Hua Zheng).

H. Zheng, Y. Yan, Y. Wang, X. Shen and C. Lu are with the Department of Electronic and Information Engineering, The Hong Kong Polytechnic University, Kowloon, Hong Kong, China (email: hua.zheng@polyu.edu.hk).

to process a 100×21800 image benefiting from GPU acceleration, making it potentially useful for real-time data processing of long-range BOTDA.

II. PRINCIPLE

A. Architecture of fastDVDnet

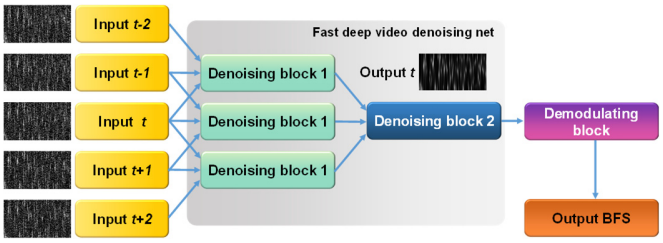

Fig. 1. The diagram of the basic architecture of fastDVDnet. The model has a two-step denoising architecture. Five consecutive frames are used as inputs of the model to denoise the central frame.

Fig. 1. displays the diagram of the basic architecture of fastDVDnet [30]. The model has a two-step denoising architecture. Comparing with one-step denoising, this architecture could effectively employ the information existent in the temporal neighbors and enforce the temporal correlation of the remaining noise in output frames. When denoising a given frame at time t, its four neighboring frames are also taken as inputs, i.e. I_{t-2}, I_{t-1}, I_t, I_{t+1}, I_{t+2}. Every three consecutive frames are fed into denoising block1 to perform denoising. Then the three outputs of denoising block1 are further denoised by denoising block2. After denoising, the central denoised frame is sent into a demodulating block to acquire BFS information. All the denoising blocks have the same architecture, while three blocks in the first denoising stage (denoising block1) share the same weights, which leads to a reduction of memory requirements of the model and facilitates the training of the network.

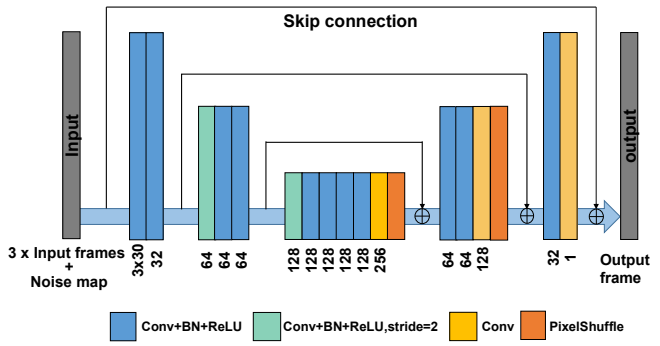

Fig. 2. The detailed architecture of denoising blocks. The feature map number is marked below each layer.

The architecture of denoising blocks is illustrated in Fig. 2. Similar to U-Net [31], it has a multi-scale encoder-decoder architecture, with skip-connections that forward the output of each one of the encoder layers directly to the input of the corresponding decoder layers. Three consecutive frames are used as input. Meanwhile, a noise map (i.e. the estimate of the noise level σ) with the same size of the input frame is also included as input, which allows the processing of spatially varying noise [32]. In the encoder layers (left side), the features of input frames are firstly extracted by two consecutive convolutional layers (kernel size=3×3, stride=1, padding=1) with batch normalization (BN) and rectified linear units (ReLU) activation. Then, convolutional layers (kernel size=3×3, padding=1) with a stride of 2 are employed to halves the size of feature maps and increase the number of filters to 128, which enables the network to learn more higher-level features from image data. In the decoder layers, to recover the desired image and achieve end to end training, the feature maps need to be upsampled. A common operation is using transposed convolution. However, transposed convolution has uneven overlap when the kernel size (the output window size) is not divisible by the stride. The uneven overlaps will produce a characteristic checkerboard-like pattern of varying magnitudes. To avoid the gridding artifacts, we use the PixelShuffle layer instead. This layer repacks its input of dimension $4n_{ch}\times h/2\times w/2$ into an output of size $n_{ch}\times h\times w$, where n_{ch}, h, w are the number of channels, the height, and the width, respectively. At the end of the network, a convolutional layer is used to map the 32 component feature vectors to the desired image. The total depth of fastDVDnet is 16.

B. Dataset and training

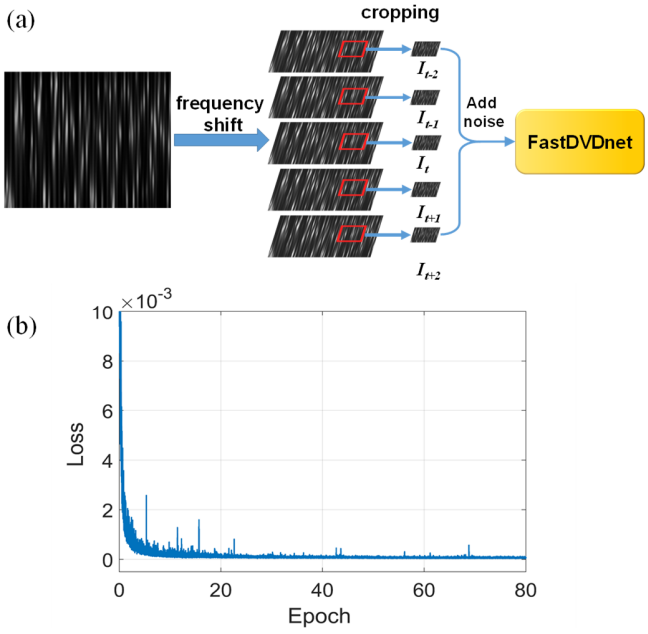

Fig. 3. (a) The schematic diagram of dataset generation. (b) Training loss as a function of epoch.

The training dataset consists of input-output pairs:

$$P_t^j = \left\{(S_t^j, M^j), I_t^j\right\}_{j=0}^{m} \quad (1)$$

Where $S_t^j = (\tilde{I}_{t-2}^j, \tilde{I}_{t-1}^j, \tilde{I}_t^j, \tilde{I}_{t+1}^j, \tilde{I}_{t+2}^j)$ is a set of noisy patches, the corresponding noise map M^j is a matrix with the same size of the patches and all its elements equal to the noisy level σ. I_t^j is the clean central patch of the sequence. Here stimulated BGSs

are used to produce the clean patches, the schematic diagram is shown in Fig. 3(a). Firstly, a frame consists of 256 BGSs with random bandwidth, frequency shift, amplitude is generated. The bandwidth of BGS is varied from 30MHz to 70MHz with a uniform distribution and the interval of amplitude is set to 0.01~0.4 according to the experimental data. Then, the subsequent frames are produced by shifting a random number BGSs of the first frame with different shift steps. 8000 sets of BGSs are generated, each set of BGSs contains 20 frames. The clean inputs (I_{t-2}, I_{t-1}, I_t, I_{t+1}, I_{t+2}) are generated by randomly cropping the stimulated BGSs at the same location in contiguous frames and the patch size is set to 96×96. While the noisy patches are produced by adding random Gaussian white noise to the ideal BGSs. The range of SNR is 2 dB to 20 dB. The loss function is

$$l(\theta)=\frac{1}{2m}\sum_{j=1}^{m}\left\|\hat{I}_t^j-I_t^j\right\|^2 \tag{2}$$

Where $\hat{I}_t^j=\mathcal{F}((S_t^j,M^j);\theta)$ is the output of the network and θ is the set of all learnable parameters. The network is implemented in PyTorch. The ADAM algorithm is applied to minimize the loss function, with all its hyper-parameters set to their default values. The number of epochs is set to 80, and the mini-batch size is 16. The learning rate is set to 1e-3 for the first 50 epochs, then changes to 1e-4 for the following 10 epochs and switches to 1e-5 for the remaining of the training. It is trained on a computer with an AMD Ryzen 4800H 8-core processor and an Nvidia GeForce GTX 2060 GPU. The training loss is shown in Fig. 3(b) and the training process takes about 5 hours and 25 minutes.

C. *BFS demodulating block*

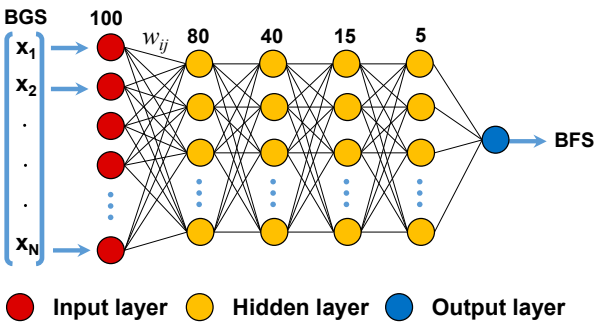

Fig. 4. The structure of BFS demodulating block.

To further speed up the entire demodulation process, a deep neural network (DNN) rather than Lorentz curve fitting (LCF) is used to extract the BFS from the denoised image [33], [34]. The structure of the DNN is shown in Fig. 4, which contains one input layer, four hidden layers, and one output layer. The number of nodes of each layer is set to 100, 80, 40, 15, 5, 1, respectively. Each node of the DNN represents a neuron and the connecting line represents a synapse with a weight of w_{ij}. The output of a neuron can be expressed as:

$$y_j=f_j(\sum w_{ij}\cdot x_i-\theta_j) \tag{3}$$

where y_j is the output of the j_{th} neuron in current layer, f_j is the activation function, w_{ij} is the weight of synapse between the i_{th} neuron in the previous layer and the j_{th} neuron in the current layer, x_i is the output of the i_{th} neuron in the previous layer, θ_j is a constant bias. Vector x (x_1 , x_2 ,..., x_N) represents the input BGS. The DNN is trained with 40000 BGS with an SNR range of 10 dB to 20 dB by using error back-propagation (BP) algorithm.

III. Experimental Setup

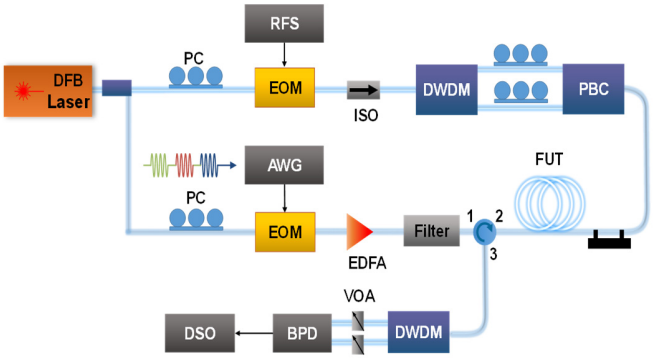

Fig. 5. Experimental setup. PC: polarization controller, EOM: electro-optic modulator, RFS: radio frequency synthesizer, AWG: arbitrary waveform generator, EDFA: Erbium-doped fiber amplifier, ISO: isolator, FUT: fiber under test, DWDM: dense wavelength division multiplexer, PBC: polarization beam combiner, VOA: variable optical attenuator, BPD, balanced photodetector, DSO: digital storage oscilloscope.

The experimental setup is shown in Fig. 5. The output of a narrow linewidth laser operating at 1549.2 nm is split into two branches by using a 50:50 coupler. In the lower branch, a high extinction ratio (> 40 dB) electro-optic modulator (EOM) and an arbitrary waveform generator (AWG) are employed to generate pump pulses with 20 ns pulse width (corresponding to a spatial resolution of 2 m). In order to fast scan the Brillouin spectral response, the frequency of the pump is swept from 250 MHz to 448 MHz with a step of 2 MHz by using the frequency-agile technique. In this way, the BGS can be reconstructed by using a low bandwidth AWG and reduce the cost of system. Pump pulses are amplified by an erbium-doped fiber amplifier (EDFA) and followed by an optical band-pass filter (BPF) to filter out the amplified spontaneous emission (ASE) noise. The power of pump pulses is carefully adjusted to avoid four-wave mixing.

On the other hand, the upper branch is used to generate a dual-sideband probe lightwave by another EOM and radio frequency synthesizer (RFS). The output frequency of RFS is set to 11.18 GHz for static testing, while 11.24 GHz for dynamic measurement. To suppress the polarization-dependent gain fluctuation, the two sidebands of the probe are separated by using a dense wavelength division multiplexer (DWDM) [20], [35], [36]. Their polarization state is adjusted to be orthogonal and recombine through a polarization beam combiner (PBC). After interacting with the pump pulses in fiber under test (FUT), the upper and lower sidebands of the probe wave are separated by DWDM again and detected by a balanced photodetector (BPD) with 200-MHz bandwidth. The electrical signals output from the PD are collected by a digital storage oscilloscope (DSO) and the acquired data are sent to a computer

for further processing. 10 km single-mode fiber whose BFS is around 10.826 GHz at room temperature is served as FUT.

IV. Experimental Results

A. Static measurement

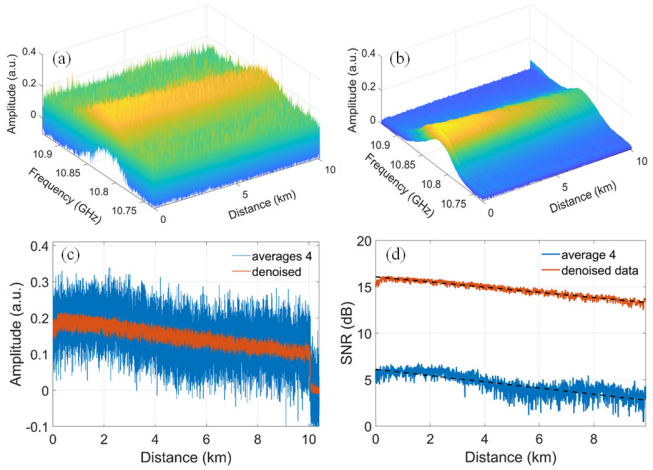

Fig. 6. (a) Raw BGS distribution along FUT (4 averages). (b) Denoised BGS by applying fastDVDnet. (c) The Brillouin time trace before (blue line) and after (red line) denoising. (d) The SNR of Brillouin time trace in (c) before (blue line) and after (red line) denoising. The black dashed lines show linear fitting (in dB scale) of the SNR curves versus distance.

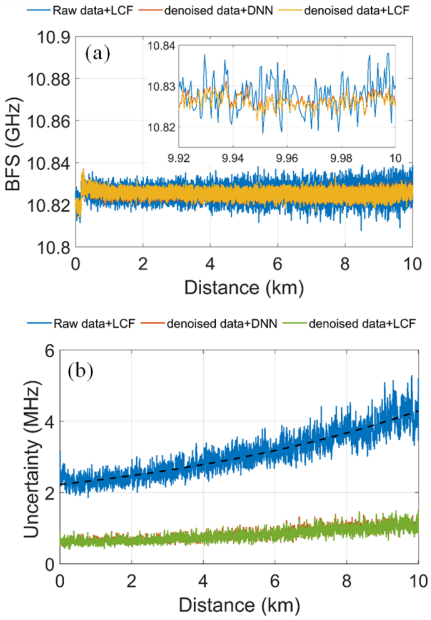

Fig. 7. (a) The demodulated BFS along sensing fiber. The blue line is derived from raw data (4 averages) by using LCF. The red line and yellow lines are derived from the denoised data using DNN and LCF, respectively. (b) The BFS uncertainty of raw data (blue line) and denoised data (red line and green line) as a function of fiber length. The black dashed lines show exponential curve fitting of the SNR curves versus distance.

To verify the denoising performance of fastDVDnet, a static test is firstly carried out. 48 consecutive frames of 2D BGS are measured, the traces are averaged 4 times. Figure 6(a) shows one of the BGS and the denoised result is shown in Fig. 6(b). Fig. 6(c) compares the raw noisy traces (blue lines) and the ones denoised (red lines) by fastDVDnet. The figure points out that a large amount of noise is removed from the raw noisy measurements, resulting in a significant increase in the contrast of the BOTDA traces. Fig. 6(d) shows the SNR of raw data (blue line) and denoised data (red line). The SNR is calculated by the ratio between the measured local response and the standard deviation of the noise floor (i.e. the end of trace where pump pulse is absent). The black dashed lines correspond to the respective linear fitting (in dB scale) of the SNR versus distance. The results indicate that the SNR of 2.5 dB obtained at the end of FUT from the raw data can be substantially boosted to 13.35 dB by applying fastDVDnet. The cascaded two-step denoising architecture and end-to-end training make it possible for fastDVDnet to handle motion without complicated motion estimation algorithm, therefore, reduce the runtimes. It takes only 0.038 s to denoise a 100×21800 image, which is much faster than VBM3D [37], [38] and other traditional methods [39], [40]. (The data transfer time between CPU and GPU is not included).

Fig. 7(a) depicts the acquired BFS from the raw data and denoised data by using LCF and DNN, respectively. The extracted BFSs show a similar profile, while the fluctuation of BFS obtained by denoised data is small than that of raw data, indicates a better sensing accuracy. To verify the performance of DNN, BFS of denoised data is also demodulated by LCF as shown in Fig. 7(a) inset. The results show the same precision, whereas DNN only takes 0.001s to extract BFS from 21800 BGSs. The BFS uncertainty is also evaluated by calculating the BFS standard deviation of 12 times continuous measurement as shown in Fig. 7(b). The frequency uncertainty of 4.3MHz obtained with the raw data at 10 km distance can be effectively improved down to 1.19 MHz.

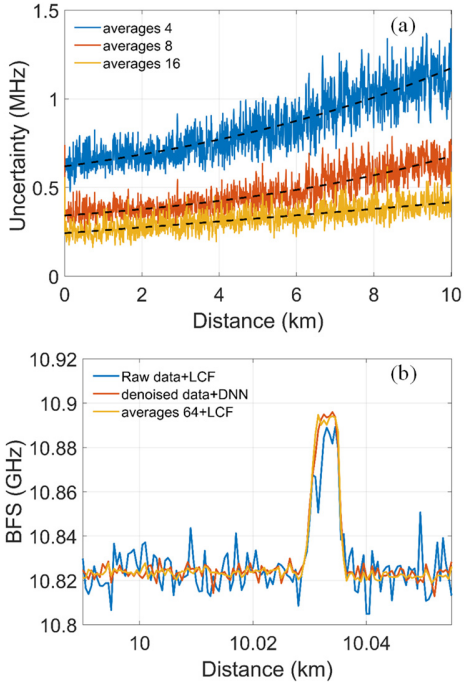

Fig. 8. (a) The BFS uncertainty with different averages. (b) BFS profiles around an 8 m-long stretched section located near the far end of FUT. The blue line is derived from raw data (4 averages) by using LCF, the red line is derived from denoised data (denoised by using fastDVDnet) by using DNN and the yellow is a reference BFS profile retrieved from measurements of 64 averages.

Different from the previous video denoising network [41] which is usually tailored to a specific noise level, fastDVDnet is trained with various noise levels, thus capable to handle different noise levels with a single network. Fig. 8(a) depicts the calculated BFS uncertainty with different average times. When the average time increases to 16, the BFS uncertainty can be effectively reduced to 0.4 MHz, at the expense of sensing speed. In order to verify that the fastDVDnet does not penalize the spatial resolution, an 8-m section of fiber at 10-km distance is stretched by two translation stages to apply strain. The BFS profiles around the strain location obtained from the raw data, denoised data and averaged data are compared as shown in Fig. 8(b). The results demonstrate that the applied fastDVDnet has little impact on the spatial resolution of the sensor.

B. *Dynamic measurement*

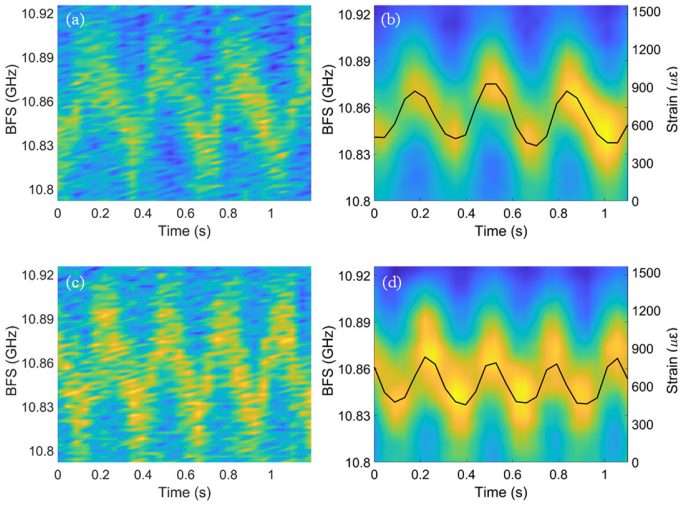

Fig. 9. The measured BGS as a function of time at the vibrated section of fiber with a driving voltage of (a) 1.2 V (raw data, 4 averages), (b) 1.2 V (denoised data), (c) 1.4 V (raw data, 4 averages), (d) 1.4 V (denoised data).

In vibration measurement, a section of 2 m fiber at the far end is stretched by two translation stages. An electric-motor-driven eccentric wheel is used to vibrate the fiber to provide periodic strain. Fig. 9(a) shows the evolution of BGS at the vibrated section when the driving voltage of the motor is 1.2 V and Fig. 9(b) is the denoising result. From Fig. 9(b) the vibration signal can be clearly observed, the period and amplitude are 0.308 s and 726 με, respectively. The higher frequency vibration signal is demonstrated by raising the driving voltage to 1.4 V, as shown in Fig. 9 (d). Signal up to 11.5 Hz is expected to be measured as the effective sampling rate of the system is 23 Hz.

To determine the accurate vibration frequency, the vibration signals in Fig. 9 are analyzed by using the Fast Fourier Transform (FFT), the frequency domain spectrum is shown in Fig. 10. The fundamental frequency of 3.25 Hz and 4 Hz can be identified.

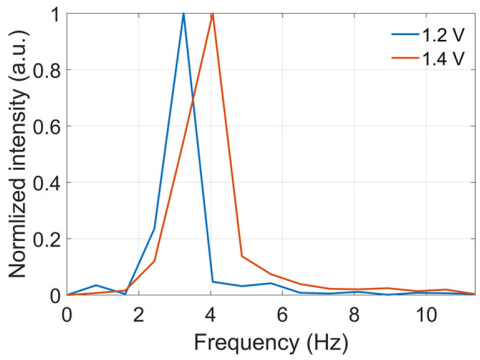

Fig. 10. Frequency-domain normalized power spectrum of vibration signals in Fig. 9.

C. *Comparison with 2D denoising CNN*

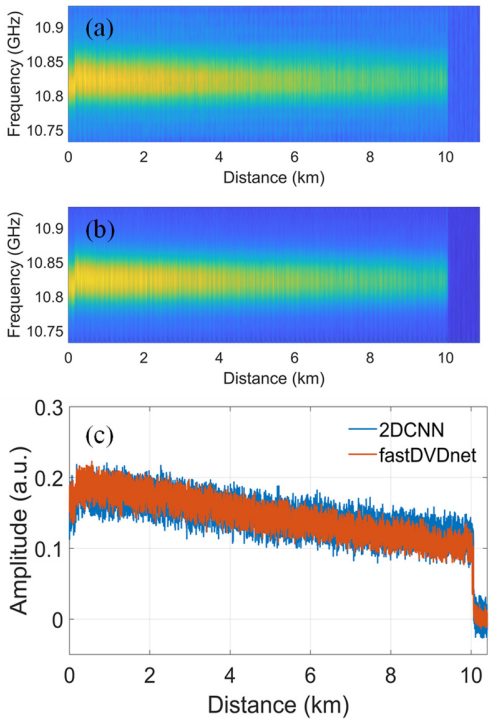

Fig. 11. Denoised BGS by using (a) 2D denoising CNN, (b) fastDVDnet, (c) Denoised Brillouin time trace by using 2D denoising CNN (blue line) and fastDVDnet (red line).

Comparing with conventional 2D denoising algorithms, the 3D denoising CNN could effectively exploit the temporal redundancy in adjacent data, which is expected to have a better performance. To fairly compare 2D denoising CNN and fastDVDnet, we modified a denoising block of fastDVDnet as a 2D denoising CNN. The modified model takes one frame as input and is trained with clean-noisy patches from the same dataset. Fig. 11 (a) and (b) show the denoised BGS distribution along sensing fiber by using 2D denoising CNN and fastDVDnet, respectively. Fig. 11(c) compares the denoised Brillouin time traces at the peak gain frequency. It can be seen that the trace processed by using 2D CNN is noisier. By using fastDVDnet, the SNR is improved about 3.6 dB.

V. Conclusion

Engineering structures have always been susceptible to various kinds of damage (deterioration, degradation, corrosion, fatigue, etc.) during their service life due to environmental, operational, and human-induced factors. Thus, the civil structures need to be inspected regularly to remain operational and protect human lives. However, with their relatively large size, damage inspection of civil infrastructure was commonly expensive. Vibration-based damage detection methods could assess the overall performance of the monitored structure, which has become one of the most important automated structural health monitoring (SHM) techniques. In this paper, we developed a scheme of long-range fast BOTDA for vibration measurement. By exploiting fastDVDnet, the SNR is greatly improved. Dynamic Brillouin sensing is realized over 10 km single-mode fiber with a sampling rate of 23 Hz, 2 m spatial resolution, and 1.19 MHz accuracy. Moreover, benefiting from GPU computing, the measured data can be denoising and demodulated in 0.038 s, which is much faster than traditional algorithms. The proposed scheme may potentially use for real-time remote monitoring of large-scale infrastructure.

References

[1] A. Barrias, J. R. Casas, and S. Villalba, "A review of distributed optical fiber sensors for civil engineering applications," *Sensors*, vol. 16, no. 5, p. 748, 2016.

[2] F. Ansari, "Practical implementation of optical fiber sensors in civil structural health monitoring," *Journal of intelligent material systems and structures*, vol. 18, no. 8, pp. 879–889, 2007.

[3] X. Ye, Y. Su, and J. Han, "Structural health monitoring of civil infrastructure using optical fiber sensing technology: A comprehensive review," *The Scientific World Journal*, vol. 2014, 2014.

[4] T. Horiguchi and M. Tateda, "BOTDA-nondestructive measurement of single-mode optical fiber attenuation characteristics using Brillouin interaction: theory," *Journal of lightwave technology*, vol. 7, no. 8, pp. 1170–1176, 1989.

[5] W. Li, X. Bao, Y. Li, and L. Chen, "Differential pulse-width pair BOTDA for high spatial resolution sensing," *Optics express*, vol. 16, no. 26, pp. 21616–21625, 2008.

[6] M. A. Soto, G. Bolognini, F. Di Pasquale, and L. Thévenaz, "Simplex-coded BOTDA fiber sensor with 1 m spatial resolution over a 50 km range," *Optics letters*, vol. 35, no. 2, pp. 259–261, 2010.

[7] D. Ba *et al.*, "Distributed measurement of dynamic strain based on multi-slope assisted fast BOTDA," *Optics express*, vol. 24, no. 9, pp. 9781–9793, 2016.

[8] D. Zhou *et al.*, "Slope-assisted BOTDA based on vector SBS and frequency-agile technique for wide-strain-range dynamic measurements," *Optics express*, vol. 25, no. 3, pp. 1889–1902, 2017.

[9] G. Yang, X. Fan, and Z. He, "Strain dynamic range enlargement of slope-assisted BOTDA by using Brillouin phase-gain ratio," *Journal of Lightwave Technology*, vol. 35, no. 20, pp. 4451–4458, 2017.

[10] H. Zheng *et al.*, "Distributed vibration measurement based on a coherent multi-slope-assisted BOTDA with a large dynamic range," *Optics letters*, vol. 44, no. 5, pp. 1245–1248, 2019.

[11] C. Jin *et al.*, "Scanning-free BOTDA based on ultra-fine digital optical frequency comb," *Optics Express*, vol. 23, no. 4, pp. 5277–5284, 2015.

[12] C. Jin *et al.*, "Single-measurement digital optical frequency comb based phase-detection Brillouin optical time domain analyzer," *Optics express*, vol. 25, no. 8, pp. 9213–9224, 2017.

[13] J. Fang, P. Xu, Y. Dong, and W. Shieh, "Single-shot distributed Brillouin optical time domain analyzer," *Optics Express*, vol. 25, no. 13, pp. 15188–15198, 2017.

[14] D. Zhou *et al.*, "Single-shot BOTDA based on an optical chirp chain probe wave for distributed ultrafast measurement," *Light: Science & Applications*, vol. 7, no. 1, pp. 1–11, 2018.

[15] Y. Dong *et al.*, "150 km fast BOTDA based on the optical chirp chain probe wave and Brillouin loss scheme," *Optics letters*, vol. 43, no. 19, pp. 4679–4682, 2018.

[16] B. Wang *et al.*, "High-performance optical chirp chain BOTDA by using a pattern recognition algorithm and the differential pulse-width pair technique," *Photonics Research*, vol. 7, no. 6, pp. 652–658, 2019.

[17] Y. Peled, A. Motil, and M. Tur, "Fast Brillouin optical time domain analysis for dynamic sensing," *Optics express*, vol. 20, no. 8, pp. 8584–8591, 2012.

[18] Y. Dong *et al.*, "High-spatial-resolution fast BOTDA for dynamic strain measurement based on differential double-pulse and second-order sideband of modulation," *IEEE Photonics Journal*, vol. 5, no. 3, pp. 2600407–2600407, 2013.

[19] I. Sovran, A. Motil, and M. Tur, "Frequency-scanning BOTDA with ultimately fast acquisition speed," *IEEE Photonics Technology Letters*, vol. 27, no. 13, pp. 1426–1429, 2015.

[20] H. Zheng *et al.*, "Polarization independent fast BOTDA based on pump frequency modulation and cyclic coding," *Optics express*, vol. 26, no. 14, pp. 18270–18278, 2018.

[21] M. A. Soto, J. A. Ramirez, and L. Thevenaz, "Intensifying the response of distributed optical fibre sensors using 2D and 3D image restoration," *Nature communications*, vol. 7, no. 1, pp. 1–11, 2016.

[22] S. Zaslawski, Z. Yang, and L. Thévenaz, "On the 2D post-processing of Brillouin optical time-domain analysis," *Journal of Lightwave Technology*, vol. 38, no. 14, pp. 3723–3736, 2020.

[23] H. Wu, L. Wang, Z. Zhao, N. Guo, C. Shu, and C. Lu, "Brillouin optical time domain analyzer sensors assisted by advanced image denoising techniques," *Optics express*, vol. 26, no. 5, pp. 5126–5139, 2018.

[24] H. Zheng, J. Zhang, H. Wu, N. Guo, and T. Zhu, "Single shot OCC-BOTDA based on polarization diversity and image denoising," *Optics and Lasers in Engineering*, vol. 137, p. 106368, 2021.

[25] B. Wang, L. Wang, C. Yu, and C. Lu, "Long-distance BOTDA sensing systems using video-BM3D denoising for both static and slowly varying environment," *Optics express*, vol. 27, no. 25, pp. 36100–36113, 2019.

[26] M. A. Soto, J. A. Ramírez, and L. Thévenaz, "Optimizing image denoising for long-range Brillouin distributed fiber sensing," *Journal of Lightwave Technology*, vol. 36, no. 4, pp. 1168–1177, 2017.

[27] M. A. Soto, J. A. Ramírez, and L. Thévenaz, "200 km fiber-loop conventional Brillouin distributed sensor with 2m spatial resolution using image denoising," in *Asia-Pacific Optical Sensors Conference*, 2016, pp. Th3A-4.

[28] H. Wu *et al.*, "Real-time denoising of Brillouin optical time domain analyzer with high data fidelity using convolutional neural networks," *Journal of Lightwave Technology*, vol. 37, no. 11, pp. 2648–2653, 2018.

[29] Y. Chang, H. Wu, C. Zhao, L. Shen, S. Fu, and M. Tang, "Distributed Brillouin frequency shift extraction via a convolutional neural network," *Photonics Research*, vol. 8, no. 5, pp. 690–697, 2020.

[30] M. Tassano, J. Delon, and T. Veit, "Fastdvdnet: Towards real-time deep video denoising without flow estimation," in *Proceedings of the IEEE/CVF Conference on Computer Vision and Pattern Recognition*, 2020, pp. 1354–1363.

[31] O. Ronneberger, P. Fischer, and T. Brox, "U-net: Convolutional networks for biomedical image segmentation," in *International Conference on Medical image computing and computer-assisted intervention*, 2015, pp. 234–241.

[32] K. Zhang, W. Zuo, and L. Zhang, "FFDNet: Toward a fast and flexible solution for CNN-based image denoising," *IEEE Transactions on Image Processing*, vol. 27, no. 9, pp. 4608–4622, 2018.

[33] B. Wang, L. Wang, N. Guo, Z. Zhao, C. Yu, and C. Lu, "Deep neural networks assisted BOTDA for simultaneous temperature and strain measurement with enhanced accuracy," *Optics express*, vol. 27, no. 3, pp. 2530–2543, 2019.

[34] B. Wang, N. Guo, L. Wang, C. Yu, and C. Lu, "Robust and fast temperature extraction for Brillouin optical time-domain analyzer by using denoising autoencoder-based deep neural networks," *IEEE Sensors Journal*, vol. 20, no. 7, pp. 3614–3620, 2019.

[35] J. Urricelqui, F. López-Fernandino, M. Sagues, and A. Loayssa, "Polarization diversity scheme for BOTDA sensors based on a double

orthogonal pump interaction," *Journal of Lightwave Technology*, vol. 33, no. 12, pp. 2633–2638, 2015.

[36] A. Lopez-Gil, A. Dominguez-Lopez, S. Martin-Lopez, and M. Gonzalez-Herraez, "Simple method for the elimination of polarization noise in BOTDA using balanced detection and orthogonal probe sidebands," *Journal of Lightwave Technology*, vol. 33, no. 12, pp. 2605–2610, 2014.

[37] D. Kostadin, F. Alessandro, and E. Karen, "Video denoising by sparse 3d transform-domain collaborative filtering," in *European signal processing conference*, 2007, vol. 149.

[38] M. Maggioni, G. Boracchi, A. Foi, and K. Egiazarian, "Video denoising using separable 4D nonlocal spatiotemporal transforms," in *Image Processing: Algorithms and Systems IX*, 2011, vol. 7870, p. 787003.

[39] H. Ji, C. Liu, Z. Shen, and Y. Xu, "Robust video denoising using low rank matrix completion," in *2010 IEEE Computer Society Conference on Computer Vision and Pattern Recognition*, 2010, pp. 1791–1798.

[40] M. Mahmoudi and G. Sapiro, "Fast image and video denoising via nonlocal means of similar neighborhoods," *IEEE signal processing letters*, vol. 12, no. 12, pp. 839–842, 2005.

[41] A. Davy, T. Ehret, J.-M. Morel, P. Arias, and G. Facciolo, "A non-local CNN for video denoising," in *2019 IEEE International Conference on Image Processing (ICIP)*, 2019, pp. 2409–2413.